JACS
JOURNAL OF THE AMERICAN CHEMICAL SOCIETY
Article
pubs.acs.org/JACS

Substrate-Mediated C−C and C−H Coupling after Dehalogenation

Huihui Kong,[†] Sha Yang,[‡] Hongying Gao,[*,†,§,∥] Alexander Timmer,[§,∥] Jonathan P. Hill,[⊥] Oscar Díaz Arado,[§,∥] Harry Mönig,[§,∥] Xinyan Huang,[†] Qin Tang,[†] Qingmin Ji,[†] Wei Liu,[*,‡] and Harald Fuchs[*,†,§,∥]

[†]Herbert Gleiter Institute of Nanoscience, and [‡]School of Materials Science and Engineering, Nanjing University of Science and Technology, Xiaolingwei 200, Nanjing 210094, Jiangsu, P. R. China

[§]Physikalisches Institut, Westfälische Wilhelms-Universität Münster, Wilhelm-Klemm-Strasse 10, 48149 Münster, Germany

[∥]Center for Nanotechnology (CeNTech), Westfälische Wilhelms-Universität Münster, Heisenbergstrasse 11, 48149 Münster, Germany

[⊥]Center for Materials Nanoarchitectonics (MANA), National Institute for Materials Science (NIMS), Namiki 1-1, Tsukuba, Ibaraki 305-0044, Japan

Supporting Information

ABSTRACT: Intermolecular C−C coupling after cleavage of C−X (mostly, X = Br or I) bonds has been extensively studied for facilitating the synthesis of polymeric nanostructures. However, the accidental appearance of C−H coupling at the terminal carbon atoms would limit the successive extension of covalent polymers. To our knowledge, the selective C−H coupling after dehalogenation has not so far been reported, which may illuminate another interesting field of chemical synthesis on surfaces besides *in situ* fabrication of polymers, i.e., synthesis of novel organic molecules. By combining STM imaging, XPS analysis, and DFT calculations, we have achieved predominant C−C coupling on Au(111) and more interestingly selective C−H coupling on Ag(111), which in turn leads to selective synthesis of polymeric chains or new organic molecules.

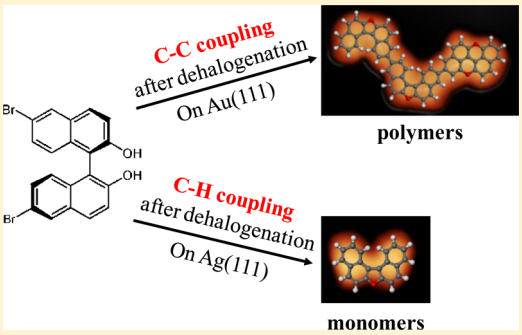

1. INTRODUCTION

Surface-assisted synthesis has received wide attention due to its potential for the creation of novel functional organic molecules and precise construction of well-defined robust architectures with the prospect of nanomaterials and nanodevices.[1−3] For such studies, scanning tunneling microscopy (STM) in combination with X-ray photoemission spectroscopy (XPS) have proven to be an excellent toolkit which allows a direct, real-space topographic identification and detailed analysis of the chemical information on both reactants and products.[1,4−7] In recent years, a series of on-surface intermolecular reactions have been mainly focused on generating distinct nanostructures, including polymeric chains and porous organic networks.[3−17] Besides the *in situ* fabrication of polymers, another interesting field of chemical synthesis, i.e., the synthesis of small organic molecules via on-surface reaction with specific regioselectivity, has been less studied, which has yet exhibited great potential for the synthesis of novel molecules with excellent selectivity and purity.[1,18−23]

As a well-known model system for surface-assisted synthesis, intermolecular C−C coupling after cleavage of C−X (usually, X = Br or I) bonds has been extensively studied. Such reactions facilitate the synthesis of polymeric nanostructures, especially various graphene nanoribbons with specific edges and latitudes,[24−27] while the accidental appearance of C−H coupling at the terminal carbon atoms would limit the successive extension of covalent polymers and facilitate the formation of small oligomers. To our knowledge, selective C−H coupling after dehalogenation has not yet been reported. Therefore, it is of great interest to study the possibility for unique C−H coupling, which leads to the effective and efficient synthesis of pure organic molecules.

To conduct the selective C−H coupling and synthesis of organic molecules, the strategy in this study is to design a precursor molecule with multiple chemically active sites (including, among others, C−X functional groups). The purpose of such a strategy is that the byproducts from other chemical reaction processes could provide an efficient hydrogen source for the C−H coupling after dehalogenation. According to previous investigations, both C−H[28] (original C−H bonds in precursor molecules) and O−H bonds[29,30] can be cleaved on metal surfaces to generate hydrogen atoms. Therefore, these should be able to serve as potential hydrogen sources. Unfortunately, C−Br bonds exhibit smaller binding energies than C−H bonds and are thus more easily activated, with intermolecular C−C coupling often occurring before breakage of C−H bonds.[24−26] This strongly indicates that C−H

Received: October 19, 2016
Published: February 10, 2017

DOI: 10.1021/jacs.6b10936
J. Am. Chem. Soc. 2017, 139, 3669−3675

functional groups are not a good choice as hydrogen source. Therefore, in this study we introduce O−H functional groups as the hydrogen donors for C−H coupling and thus select the (*R*)-(−)-6,6′-dibromo-1,1′-bi-2-naphthol (DN) molecule (see Scheme 1) as a precursor of the reaction. For such a molecule,

Scheme 1. Schematic Illustration of the Controllable C−C or C−H Coupling of the (*R*)-(−)-6,6′-Dibromo-1,1′-bi-2-naphthol (DN) Molecule on Different Surfaces

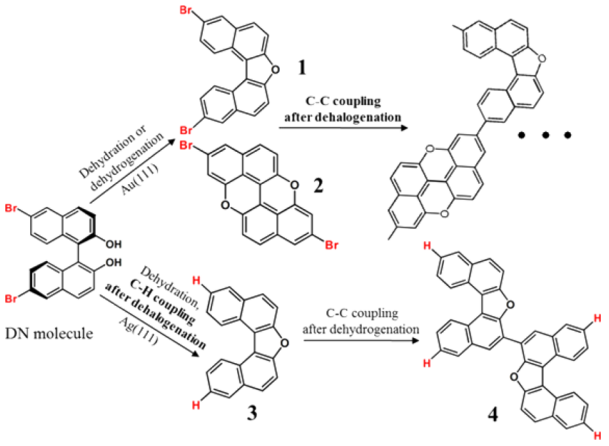

C−Br groups are prerequisite to study the C−H coupling after dehalogenation, while O−H groups could dehydrate or dehydrogenate to provide hydrogen atoms for C−H coupling. By the combination of high resolution STM imaging and state-of-the-art density functional theory (DFT) calculations and XPS analysis, we have systematically studied on-surface reactions of DN molecules on different surfaces (Scheme 1). C−C coupling is predominantly achieved on Au(111) after dehalogenation, where polymeric chains are synthesized. More interestingly, selective C−H coupling is successfully achieved on Ag(111) after dehalogenation, which subsequently leads to the synthesis of organic molecular monomers. The key to make this unique C−H coupling successful appears to be the simultaneous dehalogenation reaction and the formation of furan, which may make the hydrogen atoms produced during its formation directly diffuse to the carbon radicals where the hydrogen transfer takes place.

2. METHODS

STM, XPS and mass spectroscopy. STM experiments were performed in a UHV chamber (base pressure 1×10^{-10} mbar) equipped with the low-temperature Omicron or JT-STM held at 77 K, a molecular evaporator, and other standard facilities for sample preparation. XPS experiments were carried out in a UHV chamber, which was directly connected to the Omicron STM. The Au(111) and Ag(111) substrate were prepared by several cycles of 1.5 keV Ar^+ sputtering followed by annealing at temperatures of 770 and 700 K for 15 min, resulting in clean and flat terraces separated by monatomic steps. The DN molecules (purchased from Tokyo Chemical Industry Co., Ltd. purity >98%) were loaded into a quartz crucible in the molecular evaporator. After a thorough degassing, the DN molecules were deposited onto the clean surfaces held at room temperature. Most of the STM images were obtained with a tunneling current of 0.05 nA and sample bias of 500 mV, except where indicated otherwise. The typical width of the terraces obtained for both Au(111) and Ag(111) surfaces was around 100 nm.

Mass spectrometry measurements were carried out on an EPIC 1000 mass spectrometer (Hiden Analytical) operated in its standard mode. Such a device was directly connected to the Omicron STM system, allowing an *in situ* analysis of the sublimation process.

DFT calculations. The DFT calculations were carried out in the numeric atom-centered basis set all-electron code FHI-aims,[31] together with the Perdew−Burke−Ernzerhof (PBE) exchange-correlation functional.[32] The PBE + vdW^{surf} method[33] was employed to account for the van der Waals (vdW) interactions and collective response effects. The PBE + vdW^{surf} method extends pairwise vdW approaches to modeling of adsorbates on surfaces by a synergetic combination of the PBE + vdW method[34] for intermolecular interactions with the Lifshitz−Zaremba−Kohn theory[35,36] for the nonlocal Coulomb screening within the bulk. The atomic zeroth-order regular approximation[37] was used to treat relativistic effects for Cu atoms. The "tight" settings including the "tier2" standard basis set in the FHI-aims code were used for light elements (H, C, and O) and "tier1" for Au, Ag, and Br. A convergence criterion of 0.02 eV/Å for the maximum final force was used for structural relaxations. Also convergence criteria of 10^{-5} electrons per unit volume for the charge density and 10^{-4} eV for the total energy of the system were utilized for all computations. The Ag(111) and Au(111) surfaces were modeled by 3-layer slabs. The bottom metal layer was constrained whereas the two uppermost two metal layers and molecules were allowed to fully relax during the geometry relaxations. Different slabs were separated by more than 40 Å vacuum to eliminate the interaction between periodic images. The STM simulations were carried out within the Vienna ab initio simulation package (VASP) code[38] at a bias of +0.5 V.

Synthesis. Molecules **1** and **3** were prepared following literature methods[39−41] and purified by column chromatography (SiO_2/*n*-hexane) followed by recrystallization from chloroform/methanol and tetrahydrofuran, respectively.

Molecule **1**: ^{1}H NMR (d_8-THF, 313 K, 300 MHz): δ = 9.65 (dd, 2H, ^{3}J = 9.3 Hz, ^{4}J = 1.8 Hz), 9.73 (d, 2H, ^{3}J = 8.7 Hz), 9.80 (d, 2H, ^{3}J = 9.3 Hz), 10.13 (d, 2H, ^{4}J = 1.8 Hz), 10.80 (d, 2H, ^{3}J = 9.3 Hz) ppm; ^{13}C NMR (d_8-THF, 313 K, 75 MHz): δ = 113.71, 118.02, 119.01, 127.0, 128.02, 129.45, 131.56, 132.94, 154.77 ppm; MALDI-TOF-MS (dithranol): calc'd for $C_{20}H_{10}Br_2O$: 425.91; found m/z = 424.88 [(M − H)$^+$].

Molecule **3**: ^{1}H NMR ($CDCl_3$, 298 K, 300 MHz): δ = 7.57 (t, 2H, ^{3}J = 7.5 Hz), 7.73 (t, 2H, ^{3}J = 7.2 Hz), 7.80 (d, 2H, ^{3}J = 8.7 Hz), 7.93 (d, 2H, ^{3}J = 8.7 Hz), 8.04 (d, 2H, ^{3}J = 7.8 Hz), 9.13 (d, 2H, ^{3}J = 8.4 Hz) ppm; 13C-NMR ($CDCl_3$, 298 K, 75 MHz): δ = 112.69, 119.40, 124.37, 125.60, 126.15, 128.29, 128.61, 129.46, 131.21, 154.33 ppm; MALDI-TOF-MS (dithranol): calc'd for $C_{20}H_{12}O$: 268.09; found m/z = 267.67 [M$^+$].

3. RESULTS AND DISCUSSION

Heat-induced dehydration or dehydrogenation reaction of DN molecules on Au(111). Before deposition of the DN molecules on specific substrates, we first conducted mass spectrometry experiments to verify that the molecules remain intact during the thermal sublimation. As expected, there was no structural degradation in the DN molecules before they reached the substrate (see Supporting Information, Figure S1). Deposition of DN molecules onto Au(111) held at room temperature lead to the formation of well-ordered self-assembled structures (Figure 1a). From the high resolution STM image (Figure 1b) we find that such nanostructures are composed of tetramers as building blocks, where each molecule is imaged as an ellipsoidal bright protrusion. XPS analysis further reveals that both the C−Br bonds and C−OH bonds remain intact after deposition (Figure 4a and b). DFT calculations are employed to unravel the molecular configurations. We found that the DN molecules adopt nonplanar adsorption configurations due to the intramolecular steric hindrance (Figure 1c). Furthermore, a careful inspection reveals that the herringbone reconstruction of Au(111) underneath the self-assembled nanostructures is neither modified nor lifted,

DOI: 10.1021/jacs.6b10936
J. Am. Chem. Soc. 2017, 139, 3669−3675

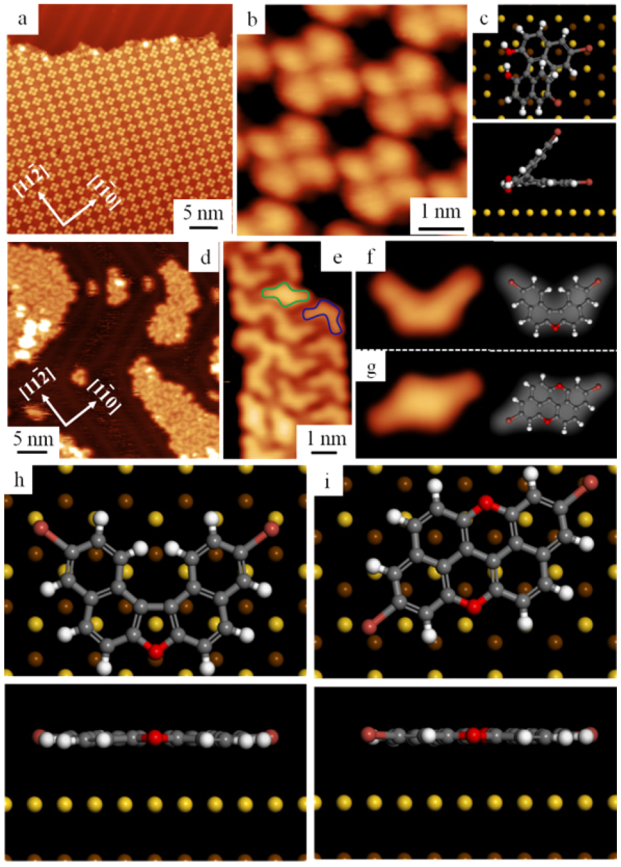

Figure 1. (a,b) Overview and high resolution STM images of the DN molecules on Au(111). (c) Top and side view models of the DN molecules adsorbed on Au(111). (d,e) Overview and high resolution STM images showing two differing species after annealing at 380 K. (f) STM image of a "V"-shaped molecule (left) and the simulated STM image (right), as well as the overlaid optimized model. (g) STM image of a parallelogram-shaped molecule (left) and the corresponding simulated STM image (right) as well as the overlaid optimized model. (h,i) Top and side view model of the "V"- and parallelogram-shaped molecules on Au(111).

indicating weak interactions between the DN molecules and the Au(111) surface.

After annealing the DN/Au(111) sample at 380 K for 30 min, structural transformation from ordered self-assembled nanostructures to irregular disordered islands is clearly recognizable (Figure 1d). The high resolution STM image shown in Figure 1e reveals that single-molecule configurations have been significantly changed compared with the state before anneal. In this case two different predominant species are identified. They are depicted by blue and green hand drawn contours (Figure 1e), which are imaged as "V"- and parallelogram-shaped molecules, respectively (also see Figure 1f and g). Furthermore, statistical analysis reveals that the ratio between molecule **1** and molecule **2** is around 10:7. Moreover, the apparent height difference between these two species and the ordered nanostructures in Figure 1a is about 2.5 Å (see Figure S2). These distinct changes in both apparent height and molecular geometry induced by the thermal treatment strongly imply that intramolecular chemical reactions should have occurred to the DN molecule, resulting in the formation of two new species.

To obtain a deeper insight into the chemical structures of these two newly synthesized species in Figure 1f and g, DFT calculations including the Au(111) substrate have been performed. In this case, multiple single-molecule products are taken into account and relaxed on the substrate. After a comparison with high resolution STM images, we find that the energetically favorable models of molecules **1** and **2** (see Scheme 1), as well as the simulated STM images, are in good agreement with the two experimentally observed newly synthesized species in both morphologies and dimensions, as shown in Figure 1f and g (also shown in Figure S3). Furthermore, molecules **1** and **2** adopt an approximately flat adsorption configuration rather than nonplanar alternatives (Figure 1h and i), which is consistent with their smaller apparent heights as compared to the DN molecules on Au(111) prior to the annealing. Based on the previous analysis, we confirm that the chemical structures of the "V"-shaped and parallelogram-shaped molecules can be attributed to molecules **1** and **2**, which are synthesized by intramolecular dehydration and dehydrogenation reactions of the DN molecules, respectively. Such an assignment could be further verified by XPS analysis, which shows C−OH groups have completely transformed into a furan group at 380 K.

Further heat-induced C−C coupling after dehalogenation on Au(111). To study the possibility of C−C coupling or C−H coupling occurring after a dehalogenation process in molecules **1** and **2**, further thermal treatment was performed. After annealing the sample at 480 K for 30 min, we observed that triangle-like islands are formed (Figure 2a). Careful

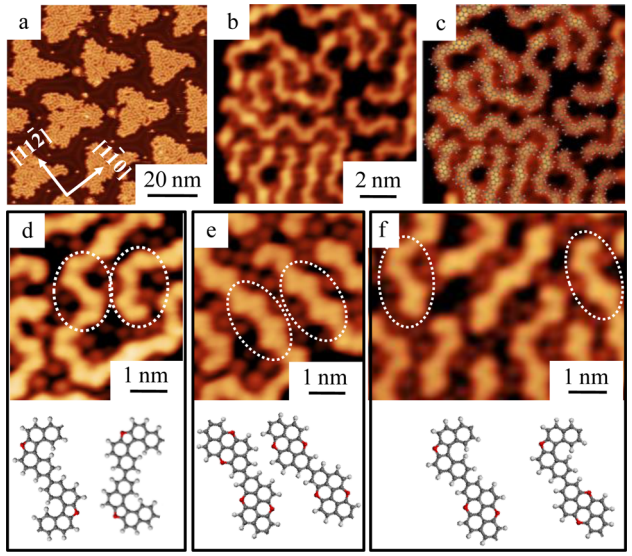

Figure 2. (a) Overview STM image showing irregular islands on Au(111) after annealing at 480 K. (b) High resolution STM image showing zigzag polymeric chains obtained by C−C coupling after dehalogenation. (c) The same STM image as (b) with the overlaid proposed model. (d−f) High resolution STM images (upper panel) and the proposed models (lower panel) showing diverse coupling constitutions.

inspection reveals that the herringbone reconstruction of Au(111) is modified, which can be attributed to the adsorption of dissociated bromine atoms on Au(111), as has been previously reported.[42] Such dissociated bromine atoms are imaged as dim spots in the corresponding high resolution STM image (Figure 2b), corroborating the dehalogenation of molecules **1** and **2**. This fact is also verified by the XPS by a pronounced chemical shift of the Br 3d peaks. The cleavage of

DOI: 10.1021/jacs.6b10936
J. Am. Chem. Soc. 2017, 139, 3669−3675

C−Br bonds further triggers the formation of a number of covalently linked zigzag chains with random directions and lengths, which are separated from each other by bromine atoms.

To account for the formation mechanism of the covalently linked zigzag chains, we perform detailed analyses on various high resolution STM images (Figure 2d−f). Such a procedure reveals that these zigzag chains are likely synthesized by intermolecular C−C coupling of the dehalogenated molecules **1** or **2** at the dehalogenated sites, including molecular homocoupling and heterocoupling, as demonstrated by the proposed model. These C−C coupling modes are further verified by the good agreement between the simulated and experimental STM images of covalent dimers (Figure S4). The high resolution STM image including a proposed model superimposed in Figure 2c illustrates the diversity of constitutions after C−C coupling. These covalent chains are found to grow in limited lengths, and their terminations are passivated by accidental C−H coupling, as evidenced by the good agreements of the experimental STM images of minor monomers and dimers with scaled optimized models as well as the simulated STM images (Figure S4). It should be nevertheless noted that the observed C−H coupling is less favored, with intermolecular C−C coupling after dehalogenation still acting as the predominant coupling type.

Heat-induced C−H coupling of DN molecules after dehalogenation on Ag(111). In the next step, we explore the controllable selection of C−H coupling by using the Ag(111) substrate to slightly modulate the reaction energy barrier for both dehydration (or dehydrogenation) and dehalogenation reaction steps. After deposition of DN molecules onto Ag(111) at RT, we observed two self-assembled nanostructures (Figure S5). After annealing this sample at 380 K for 30 min, two types of well-ordered nanostructures are mainly observed (Figure 3a and c). All the molecules in both nanostructures exist in the form of single units with identical

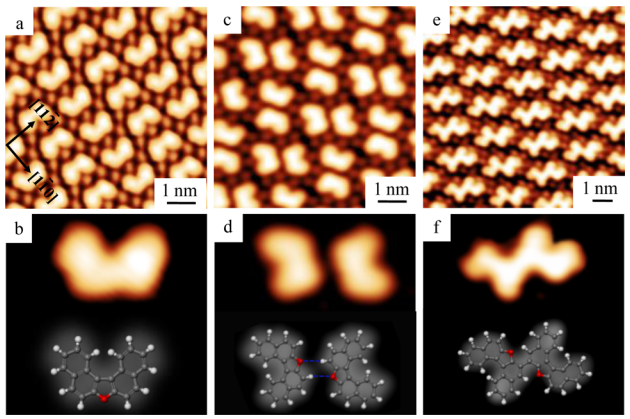

Figure 3. (a,c) STM images showing two ordered nanostructures after deposition of DN molecule on Ag(111) with post annealing at 380 K. (b) Close-up STM image (upper panel) and the simulated one (lower panel) as well as the overlaid optimized model showing the "U"-shaped molecular topography in (a). (d) Close-up STM image (upper panel) and the simulated one (lower panel) as well as the overlaid optimized model showing hydrogen-bonded dimer in (c) formed by two "U"-shaped molecules. (e) STM image showing nanostructures after annealing at 480 K. (f) Close-up STM image (upper panel) and the simulated one (lower panel) as well as the overlaid optimized model showing the covalently linked dimer in (e).

"U"-shaped molecular configurations. However, the "U"-shaped molecular monomers in Figure 3a are separated from each other by dim spots which are also, in this case, attributed to bromine atoms, while in Figure 3c two of these molecules are likely linked by noncovalent bonds to form dimers.

To gain insight into the chemical structures of the "U"-shaped molecules, DFT calculations have been performed. First, we considered the case where the chemical structure of the "U"-shaped molecules matched the one from molecules **1** or **2**, and subsequently built the corresponding models on Ag(111). By comparing the simulated STM images of molecules **1** and **2** (Figure S6) to the STM contrast of the "U"-shaped molecule, we find that neither of them correspond with the experimentally observed molecular configuration. Therefore, we ruled out these two candidates.

Alternatively, a detailed inspection revealed that the "U"-shaped molecule looks similar to molecule **1** but with shorter wings. Therefore, we believe that the "U"-shaped molecules could be assigned either to a dehalogenated molecule **1** with radicals at the tails or to molecule **3**. It is important to note that both possibilities could result in the shorter wings visible in the STM images. Therefore, we built up two models based on dehalogenated molecule **1** with carbon radicals at its tail (Figure S7) and molecule **3** (see Figure S8 and Figure 3b), respectively. After relaxation, we find that the dehalogenated molecule **1** with carbon radicals strongly interacts with the Ag(111) surface by forming C−Ag bonds and thus resulting in a bent adsorption configuration. In this case, neither the optimized models nor the simulated STM images are in agreement with the STM contrast (Figure S7). This is further supported by the XPS data for the C 1s region of DN molecules on Ag(111), where a distinct spectroscopic signature supporting a C−Ag bond formation was not observed. On the other hand, we built the model based on molecule **3** (see Scheme 1), where the carbon radicals are passivated by hydrogen atoms. Surprisingly, the optimized model and the corresponding simulated STM image of molecule **3** show very good agreement with the experimental STM images, as illustrated in Figure 3b and Figure S8. The simulated STM image of the nanostructure based on molecule **3** (Figure S9) also shows good agreement with that in Figure 3a. Furthermore, the chemical structure of molecule **3** could reasonably lead to the formation of the dimer structures in Figure 3c, where two "U"-shaped molecules are interlinked by two directional C−H···O hydrogen bonds (Figure 3d).

To further support our assumption on assigning the "U"-shaped molecule to molecule **3**, we have also *ex-situ* synthesized molecule **3** and deposited it on Ag(111). High resolution STM images (Figure S10) revealed that both the size and single-molecule configuration of the *ex-situ* synthesized molecule **3** are in good agreement with those of the "U"-shaped molecule on Ag(111). In view of such theoretical and experimental evidence, we confirm that the "U"-shaped molecules can be attributed to molecule **3**. Interestingly, the assignment of "U"-shaped molecule to molecule **3** strongly implies that we have effectively inhibited the intermolecular C−C coupling and successfully achieved the selective C−H coupling after dehalogenation by deposition of DN molecules on Ag(111) with post anneal at 380 K. Moreover, such newly formed C−H bonds remain intact upon further annealing to 480 K for 30 min (see Figure 3e). In this case, the C−H bonds close to oxygen atoms are activated, and finally molecule **4** (see Scheme 1) is synthesized, as verified by the good agreement between the experimental

DOI: 10.1021/jacs.6b10936
J. Am. Chem. Soc. 2017, 139, 3669−3675

morphology observed by STM and the optimized model and simulated STM image as shown in Figure 3f (also shown in Figure S11).

To further understand the unexpected C−H coupling of DN molecules on Ag(111), we have *ex-situ* synthesized molecule **1** and subsequently performed a control experiment on the Ag(111) surface. Since molecule **1** is the product of DN molecules after dehydration, we were interested in avoiding the influence of byproducts on the C−C or C−H coupling. After depositing molecule **1** on Ag(111) and annealing the sample at 380 K for 30 min, we found that C−Br bonds are cleaved as expected. It was surprising to note that C−C or C−Ag coupling rather than C−H coupling occurs after dehalogenation. In this case, organometallic chains or five-member rings are synthesized (Figure S12). Since the only difference between molecule **1** and DN molecule is the availability of byproducts on Ag(111), we reach the conclusion that these are the source of the hydrogen atoms that play important roles on the selective C−H coupling of DN molecules and the selective formation of molecule **3**.

XPS analysis of the reaction processes of DN molecules on Au(111) and Ag(111). To analyze the reaction process of DN molecules on Au(111) and Ag(111), and more importantly, unravel the role of OH groups on the C−H coupling of DN molecules on Ag(111), additional core-level XPS experiments have been carried out. The sample temperature dependent evolution of the Br 3d and O 1s XPS core-level spectra of DN on Au(111) and Ag(111) is shown in Figure 4.

After deposition of DN on Au(111), XPS quantification of the DN/Au(111) sample yields a surface elemental composition of 84 At% (carbon), 8 At% (oxygen), and 8 At% (bromine), which is consistent with the stoichiometry of intact DN molecules on the substrate. The spin−orbit split Br 3d doublet corresponding to the RT deposited DN molecules shows two peaks at binding energies of E_b(Br 3d $_{5/2}$) = 69.4 eV and E_b(Br 3d $_{3/2}$) = 70.4 eV, which are in good agreement with values commonly associated with C−Br bonds[43−45] and further verify our STM results shown in Figure 1a. After annealing at 380 K the intensity of the Br 3d line is significantly reduced, while the position of the two peaks remains at the same location. After further annealing to 480 K, the contribution at a higher binding energy is now absent, and sparse additional intensity appearing around $E_b \approx 67.9$ eV is observed. This is commonly attributed to Br atoms adsorbed on Au(111).[44,46] Thus, it is reasonable to conclude that the complete debromination of DN molecules occurred at around 480 K and that subsequent desorption of Br atoms through formation of Br_2 occurs although some Br atoms remain physisorbed on Au(111).

The corresponding O 1s spectra depicted in Figure 4b also show a distinct variation as a result of the stepwise thermal treatment. The spectrum corresponding to the as-deposited DN molecules can be fitted with a single peak at $E_{b[OH]}$(O 1s) = 532.7 eV. Such a contribution can be assigned to the oxygen in the hydroxyl group of the naphthol units (C−OH).[47−49] After thermal annealing above 380 K, we observe that the peak is shifted by ΔE_b = 0.4 eV to $E_{b[C-O-C]}$(O 1s) = 533.1 eV, and that the full width at half-maximum (fwhm) remains unchanged. The position of the O 1s peak appears at a slightly lower binding energy than previously reported values for furan on Ag(110). Moreover, such a position is quite similar to values reported for thin films of polyfuran or adsorption of furan with

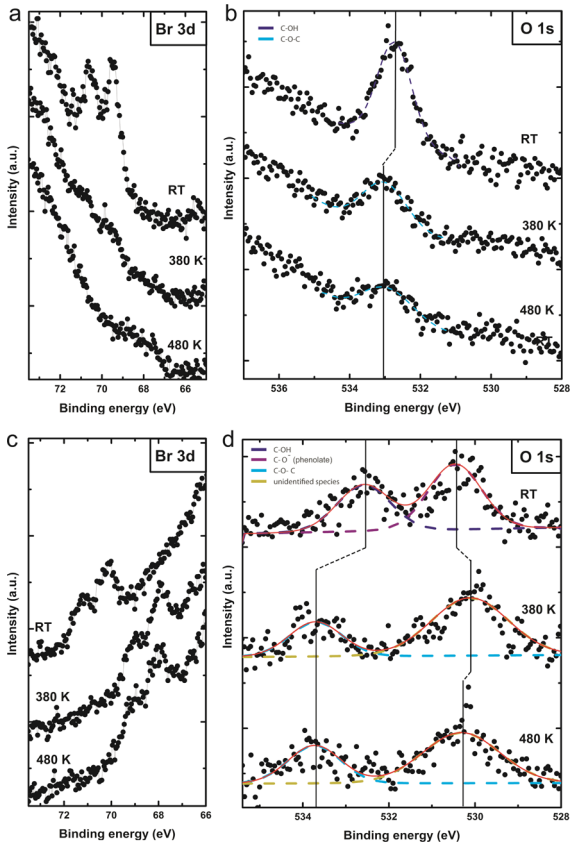

Figure 4. XP spectra and analysis of the Br 3d (a) and O 1s (b) peaks of DN molecules adsorbed on Au(111), as well as Br 3d (c) and O 1s (d) peaks on Ag(111). The corresponding annealing temperature for each sample preparation is indicated.

submonolayer coverage on other substrates.[50−54] Consequently, we ascribe this spectroscopic observation to the formation of a cyclic enol ether, i.e., furan, which is consistent with the STM results where molecules **1** or **2** are observed. After annealing at 480 K we do not observe a shift of the position of the O 1s peak despite its decreased intensity. This fact indicates that no further chemical reactions occurred to the oxygenated functional group, while the decreased intensity points toward a decrease of the surface coverage. The analysis and shape of the C 1s spectrum are also consistent with a dehalogenation and C−C coupling reaction (Figure S13).

On the other hand, the XPS data for the DN molecules on Ag(111) is depicted in Figure 4c and d. The Br 3d spectrum corresponding to the self-assembly of DN molecules on this substrate (Figure 4c) shows a spin−orbit split doublet at 70.2/71.2 eV. This feature strongly indicates that the C−Br bonds remain intact after the on-surface adsorption. After thermal annealing at 380 K, a doublet with nearly the same intensity appears at 69.0/68.0 eV, while the signal at the previous position where the peaks were observed is now absent. This indicates a complete C−Br bond cleavage of DN molecules on Ag(111) at 380 K and subsequent chemisorption of bromine.[55] Successive annealing at 480 K leads to a slight decrease of the Br 3d signal, but no significant peak shift is observed.

The O 1s region depicted in Figure 4d shows that, next to the hydroxyl-related component at $E_{b[OH]}$(O 1s) = 532.6 eV, a second peak at $E_{b[O^-]}$(O 1s) = 530.5 eV is already visible at RT on Ag(111). The second peak at a lower binding energy could be assigned to the O atom in a phenolate (C−O^-) group,

DOI: 10.1021/jacs.6b10936
J. Am. Chem. Soc. 2017, 139, 3669−3675

indicating a partial dehydrogenation of the DN molecule already occurs upon adsorption.[7,47,49] In combination with the DFT calculated model shown in Figure S5, it is likely that the OH groups closer to the surface may be dehydrogenated, probably due to the possible nonplanar adsorption configurations of the DN molecules. In the proposed reaction mechanism, the hydrogen atoms of both OH groups are designated to terminate the carbon radicals after cleavage of C−Br bonds. It should be noted that a similar substrate-mediated hydrogen transfer has also been proposed for a hydroxyphenyl-substituted porphyrin.[56] Furthermore, though atomic hydrogen can undergo recombinative desorption from a bare Ag(111) substrate, it has been clearly demonstrated that the specific interaction between the surface hydrogen and the phenoxy entity retains the hydrogen atom far above the normal desorption temperature in the case of phenol adsorbed on Al(111).[57,58] Such a specific molecule−substrate interaction could also stabilize the hydrogen atom in our case.

After annealing at 380 K the peak at higher binding energy shifts to $E_b[_{C-O-C}]$(O 1s) = 533.7 eV. Such a behavior is in very good agreement with values reported for furan adsorbed on Ag(110) and polyfuran films.[50,54] Therefore, we ascribe this peak to the oxygen atoms in the furan units after their formation. This strongly implies that dehalogenation reaction of DN molecules occurred simultaneously with the formation of the furan ring. Subsequently, the hydrogen atoms (those generated from the thermal induced dissociation of the OH groups as well as those generated already after adsorption) are likely transferred to the carbon radical and form molecule **3**. The behavior of the second O 1s peak located at a lower binding energy is initially less unambiguous, especially since the fwhm is now significantly broader. In this case the peak shifts to a lower binding energy of E_b(O 1s) = 530.1 eV and after further annealing at 480 K back up to E_b(O 1s) = 530.3 eV. However, the O 1s peak at $E_b[_{C-O-C}]$(O 1s) = 533.7 eV does not change its position. This strongly indicates that several oxygen species contribute to the spectroscopic signal at lower binding energies. It is likely that the shape of this peak originates from a coexistence of another DN species and oxygen atoms adsorbed on the silver substrate, which are known to contribute to the photoelectron intensity at $E_b \approx$ 530.0 eV.[59] By another DN species we refer, for example, to the adsorption configurations depicted in Figure S5, where two $C-O^-$ groups are bound to substrate and thus the formation of furan ring is inhibited. The shift back to slightly higher binding energies could then be the result of the change in the ratio between such two components. At the higher annealing temperature of 480 K, oxygen atoms might desorb from the Ag(111) surface, while the phenolate related signal remains unchanged. For a more detailed analysis (including the C 1s peak), see the Supporting Information (Figure S14). Finally, it is important to note that our XPS results strongly support that the final dehydrogenation reaction occurred simultaneously with the formation of the furan ring at 380 K, resulting in the formation of molecule **3** on Ag(111).

4. CONCLUSIONS

In conclusion, by means of high resolution STM imaging, XPS analysis, and DFT calculations, we have achieved selective C−C coupling or C−H coupling after on-surface dehalogenation. Subsequently, such reaction steps further induced the synthesis of predominant polymers or new organic molecules. According to our XPS experiments, the key to facilitate the unpredictable C−H coupling seems to be the simultaneous dehalogenation reaction and formation of furan rings so that the hydrogen atoms produced during the formation of furan rings can directly transfer to the carbon radicals formed due to dehalogenation. These findings extend the on-surface reactions toolbox for the bottom-up fabrication of organic nanomaterials, allowing the precise synthesis of small organic molecules by the combination of their rational design and the selection of substrates.

■ ASSOCIATED CONTENT

Supporting Information

The Supporting Information is available free of charge on the ACS Publications website at DOI: 10.1021/jacs.6b10936.

Mass spectrometry analysis, STM images, and XPS analysis (PDF)

■ AUTHOR INFORMATION

Corresponding Authors

*gaoh@uni-muenster.de
*weiliu@njust.edu.cn
*fuchsh@uni-muenster.de

ORCID

Huihui Kong: 0000-0001-5652-5269
Qingmin Ji: 0000-0001-7810-3438

Notes

The authors declare no competing financial interest.

■ ACKNOWLEDGMENTS

The authors acknowledge the financial support from the Research Fund for Postdoctoral Program of Jiangsu Province (AD41606), Science and Technology Program of Jiangsu Province (BK20151484 and AD41572). We also thank the Deutsche Forschungsgemeinschaft (SFB 858 and TRR 61) for financial support.

■ REFERENCES

(1) Otero, G.; Biddau, G.; Sanchez-Sanchez, C.; Caillard, R.; Lopez, M. F.; Rogero, C.; Palomares, F. J.; Cabello, N.; Basanta, M. A.; Ortega, J.; Mendez, J.; Echavarren, A. M.; Perez, R.; Gomez-Lor, B.; Martin-Gago, J. A. *Nature* **2008**, *454*, 865−868.

(2) de Oteyza, D. G.; Gorman, P.; Chen, Y. C.; Wickenburg, S.; Riss, A.; Mowbray, D. J.; Etkin, G.; Pedramrazi, Z.; Tsai, H. Z.; Rubio, A.; Crommie, M. F.; Fischer, F. R. *Science* **2013**, *340*, 1434−1437.

(3) Lafferentz, L.; Ample, F.; Yu, H.; Hecht, S.; Joachim, C.; Grill, L. *Science* **2009**, *323*, 1193−1197.

(4) Grill, L.; Dyer, M.; Lafferentz, L.; Persson, M.; Peters, M. V.; Hecht, S. *Nat. Nanotechnol.* **2007**, *2*, 687−691.

(5) Arado, O. D.; Monig, H.; Franke, J. H.; Timmer, A.; Held, P. A.; Studer, A.; Fuchs, H. *Chem. Commun.* **2015**, *51*, 4887−4890.

(6) Held, P. A.; Gao, H. Y.; Liu, L. C.; Muck-Lichtenfeld, C.; Timmer, A.; Monig, H.; Barton, D.; Neugebauer, J.; Fuchs, H.; Studer, A. *Angew. Chem., Int. Ed.* **2016**, *55*, 9777−9782.

(7) Urgel, J. I.; Cirera, B.; Wang, Y.; Auwarter, W.; Otero, R.; Gallego, J. M.; Alcami, M.; Klyatskaya, S.; Ruben, M.; Martin, F.; Miranda, R.; Ecija, D.; Barth, J. V. *Small* **2015**, *11*, 6358−6364.

(8) Sun, Q.; Cai, L. L.; Ma, H. H.; Yuan, C. X.; Xu, W. *ACS Nano* **2016**, *10*, 7023−7030.

(9) Weigelt, S.; Busse, C.; Bombis, C.; Knudsen, M. M.; Gothelf, K. V.; Strunskus, T.; Woll, C.; Dahlbom, M.; Hammer, B.; Laegsgaard, E.; Besenbacher, F.; Linderoth, T. R. *Angew. Chem., Int. Ed.* **2007**, *46*, 9227−9230.

(10) Jiang, L.; Papageorgiou, A. C.; Oh, S. C.; Saglam, O.; Reichert, J.; Duncan, D. A.; Zhang, Y. Q.; Klappenberger, F.; Guo, Y. Y.; Allegretti, F.; More, S.; Bhosale, R.; Mateo-Alonso, A.; Barth, J. V. *ACS Nano* **2016**, *10*, 1033−1041.

DOI: 10.1021/jacs.6b10936
J. Am. Chem. Soc. 2017, 139, 3669−3675

(11) Zwaneveld, N. A. A.; Pawlak, R.; Abel, M.; Catalin, D.; Gigmes, D.; Bertin, D.; Porte, L. *J. Am. Chem. Soc.* **2008**, *130*, 6678−6679.
(12) Zhong, D. Y.; Franke, J. H.; Podiyanachari, S. K.; Blomker, T.; Zhang, H. M.; Kehr, G.; Erker, G.; Fuchs, H.; Chi, L. F. *Science* **2011**, *334*, 213−216.
(13) Sun, Q.; Cai, L. L.; Ding, Y. Q.; Xie, L.; Zhang, C.; Tan, Q. G.; Xu, W. *Angew. Chem., Int. Ed.* **2015**, *54*, 4549−4552.
(14) Sun, Q.; Zhang, C.; Kong, H. H.; Tan, Q. G.; Xu, W. *Chem. Commun.* **2014**, *50*, 11825−11828.
(15) Cirera, B.; Zhang, Y. Q.; Bjork, J.; Klyatskaya, S.; Chen, Z.; Ruben, M.; Barth, J. V.; Klappenberger, F. *Nano Lett.* **2014**, *14*, 1891−1897.
(16) Wiengarten, A.; Seufert, K.; Auwarter, W.; Ecija, D.; Diller, K.; Allegretti, F.; Bischoff, F.; Fischer, S.; Duncan, D. A.; Papageorgiou, A. C.; Klappenberger, F.; Acres, R. G.; Ngo, T. H.; Barth, J. V. *J. Am. Chem. Soc.* **2014**, *136*, 9346−9354.
(17) Li, Q.; Yang, B.; Lin, H. P.; Aghdassi, N.; Miao, K. J.; Zhang, J. J.; Zhang, H. M.; Li, Y. Y.; Duhm, S.; Fan, J.; Chi, L. F. *J. Am. Chem. Soc.* **2016**, *138*, 2809−2814.
(18) Kruger, J.; Pavlicek, N.; Alonso, J. M.; Perez, D.; Guitian, E.; Lehmann, T.; Cuniherti, G.; Gourdon, A.; Meyer, G.; Gross, L.; Moresco, F.; Pena, D. *ACS Nano* **2016**, *10*, 4538−4542.
(19) de Oteyza, D. G.; Paz, A. P.; Chen, Y. C.; Pedramrazi, Z.; Riss, A.; Wickenburg, S.; Tsai, H. Z.; Fischer, F. R.; Crommie, M. F.; Rubio, A. *J. Am. Chem. Soc.* **2016**, *138*, 10963−10967.
(20) Amsharov, K.; Abdurakhmanova, N.; Stepanow, S.; Rauschenbach, S.; Jansen, M.; Kern, K. *Angew. Chem., Int. Ed.* **2010**, *49*, 9392−9396.
(21) Cirera, B.; Gimenez-Agullo, N.; Bjork, J.; Martinez-Pena, F.; Martin-Jimenez, A.; Rodriguez-Fernandez, J.; Pizarro, A. M.; Otero, R.; Gallego, J. M.; Ballester, P.; Galan-Mascaros, J. R.; Ecija, D. *Nat. Commun.* **2016**, *7*, 11002.
(22) Abel, M.; Clair, S.; Ourdjini, O.; Mossoyan, M.; Porte, L. *J. Am. Chem. Soc.* **2011**, *133*, 1203−1205.
(23) Heinrich, B. W.; Ahmadi, G.; Muller, V. L.; Braun, L.; Pascual, J. I.; Franke, K. J. *Nano Lett.* **2013**, *13*, 4840−4843.
(24) Cai, J. M.; Ruffieux, P.; Jaafar, R.; Bieri, M.; Braun, T.; Blankenburg, S.; Muoth, M.; Seitsonen, A. P.; Saleh, M.; Feng, X. L.; Mullen, K.; Fasel, R. *Nature* **2010**, *466*, 470−473.
(25) Chen, Y. C.; Cao, T.; Chen, C.; Pedramrazi, Z.; Haberer, D.; de Oteyza, D. G.; Fischer, F. R.; Louie, S. G.; Crommie, M. F. *Nat. Nanotechnol.* **2015**, *10*, 156−160.
(26) Chen, Y. C.; de Oteyza, D. G.; Pedramrazi, Z.; Chen, C.; Fischer, F. R.; Crommie, M. F. *ACS Nano* **2013**, *7*, 6123−6128.
(27) Ruffieux, P.; Wang, S. Y.; Yang, B.; Sanchez-Sanchez, C.; Liu, J.; Dienel, T.; Talirz, L.; Shinde, P.; Pignedoli, C. A.; Passerone, D.; Dumslaff, T.; Feng, X. L.; Mullen, K.; Fasel, R. *Nature* **2016**, *531*, 489−492.
(28) Talirz, L.; Sode, H.; Cai, J. M.; Ruffieux, P.; Blankenburg, S.; Jafaar, R.; Berger, R.; Feng, X. L.; Mullen, K.; Passerone, D.; Fasel, R.; Pignedoli, C. A. *J. Am. Chem. Soc.* **2013**, *135*, 2060−2063.
(29) Bebensee, F.; Svane, K.; Bombis, C.; Masini, F.; Klyatskaya, S.; Besenbacher, F.; Ruben, M.; Hammer, B.; Linderoth, T. *Chem. Commun.* **2013**, *49*, 9308−9310.
(30) Pawlak, R.; Clair, S.; Oison, V.; Abel, M.; Ourdjini, O.; Zwaneveld, N. A. A.; Gigmes, D.; Bertin, D.; Nony, L.; Porte, L. *ChemPhysChem* **2009**, *10*, 1032−1035.
(31) Blum, V.; Gehrke, R.; Hanke, F.; Havu, P.; Havu, V.; Ren, X.; Reuter, K.; Scheffler, M. *Comput. Phys. Commun.* **2009**, *180*, 2175.
(32) Perdew, J.; Burke, K.; Ernzerhof, M. *Phys. Rev. Lett.* **1996**, *77*, 3865.
(33) Ruiz, V. G.; Liu, W.; Zojer, E.; Scheffler, M.; Tkatchenko, A. *Phys. Rev. Lett.* **2012**, *108*, 146103.
(34) Tkatchenko, A.; Scheffler, M. *Phys. Rev. Lett.* **2009**, *102*, 073005.
(35) Lifshitz, E. M. *Sov. Phys. JETP* **1956**, *2*, 73−83.
(36) Zaremba, E.; Kohn, W. *Phys. Rev. B* **1976**, *13*, 2270.
(37) van Lenthe, E.; Baerends, E.-J.; Snijders, J. G. *J. Chem. Phys.* **1994**, *101*, 9783.
(38) Kresse, G.; Furthmuller, J. *Phys. Rev. B* **1996**, *54*, 8207−8215.
(39) Brunnstrom, G. *J. Am. Chem. Soc.* **1955**, *77*, 2463−2465.
(40) Areephong, J.; Ruangsupapichart, N.; Thongpanchang, T. *Tetrahedron Lett.* **2004**, *45*, 3067−3070.
(41) Xie, X.; Zhang, T. Y.; Zhang, Z. *J. Org. Chem.* **2006**, *71*, 6522−6529.
(42) Pham, T. A.; Song, F.; Nguyen, M. T.; Li, Z. S.; Studener, F.; Stohr, M. *Chem. - Eur. J.* **2016**, *22*, 5937−5944.
(43) Bulusheva, L. G.; Okotrub, A. V.; Flahaut, E.; Asanov, I. P.; Gevko, P. N.; Koroteev, V. O.; Fedoseeva, Y. V.; Yaya, A.; Ewels, C. P. *Chem. Mater.* **2012**, *24*, 2708−2715.
(44) Simonov, K. A.; Vinogradov, N. A.; Vinogradov, A. S.; Generalov, A. V.; Zagrebina, E. M.; Martensson, N.; Cafolla, A. A.; Carpy, T.; Cunniffe, J. P.; Preobrajenski, A. B. *J. Phys. Chem. C* **2014**, *118*, 12532−12540.
(45) Smykalla, L.; Shukrynau, P.; Korb, M.; Lang, H.; Hietschold, M. *Nanoscale* **2015**, *7*, 4234−4241.
(46) Plekan, O.; Feyer, V.; Tsud, N.; Vondracek, M.; Chab, V.; Matolin, V.; Prince, K. C. *Surf. Sci.* **2012**, *606*, 435−443.
(47) Fischer, S.; Papageorgiou, A. C.; Lloyd, J. A.; Oh, S. C.; Diller, K.; Allegretti, F.; Klappenberger, F.; Seitsonen, A. P.; Reichert, J.; Barth, J. V. *ACS Nano* **2014**, *8*, 207−215.
(48) Bowker, M.; Madix, R. J. *Surf. Sci.* **1980**, *95*, 190−206.
(49) Bowker, M.; Madix, R. J. *Surf. Sci.* **1982**, *116*, 549−572.
(50) Solomon, J. L.; Madix, R. J.; Stohr, J. *J. Chem. Phys.* **1991**, *94*, 4012−4023.
(51) Qiao, M. H.; Tao, F.; Cao, Y.; Li, Z. H.; Dai, W. L.; Deng, J. F.; Xu, G. Q. *J. Chem. Phys.* **2001**, *114*, 2766−2774.
(52) Lee, H. K.; Kim, K. J.; Kang, T. H.; Chung, J.; Kim, B. *Surf. Sci.* **2008**, *602*, 914−918.
(53) Yan, F. Q.; Qiao, M. H.; Wei, X. M.; Liu, Q. P.; Deng, J. F.; Xu, G. Q. *J. Chem. Phys.* **1999**, *111*, 8068−8076.
(54) Glenis, S.; Benz, M.; LeGoff, E.; Schindler, J. L.; Kannewurf, C. R.; Kanatzidis, M. G. *J. Am. Chem. Soc.* **1993**, *115*, 12519−12525.
(55) Wu, Y. J.; Wang, W. H.; Chiang, C. M. *Langmuir* **2002**, *18*, 1449−1452.
(56) Smykalla, L.; Shukrynau, P.; Mende, C.; Lang, H.; Knupfer, M.; Hietschold, M. *Chem. Phys.* **2015**, *451*, 39−45.
(57) Zhou, X.-L.; White, J. M.; Koel, B. E. *Surf. Sci.* **1989**, *218*, 201−210.
(58) Bartlett, B.; Valdisera, J. M.; Russell, J. N., Jr. *Surf. Sci.* **1999**, *442*, 265−276.
(59) Rehren, C.; Muhler, M.; Bao, X.; Schlögl, R.; Ertl, G. *Z. Phys. Chem.* **1991**, *174*, 11−52.

DOI: 10.1021/jacs.6b10936
J. Am. Chem. Soc. 2017, 139, 3669−3675